Ab initio study of the (0001) surfaces of hematite and chromia: Influence of strong electronic correlations

A. Rohrbach, J. Hafner,* and G. Kresse

Institut für Materialphysik and Center for Computational Materials Science, Universität Wien, Sensengasse 8/12, A-1090 Wien, Austria

We present a detailed *ab initio* investigation of the stability, the structural, electronic, and magnetic properties of the (0001) surfaces of hematite (Fe_2O_3) and chromia or eskolaite (Cr_2O_3). Strong electron correlation effects not included in a density-functional description are described by a Hubbard-type on-site Coulomb repulsion (the DFT+U approach). For bulk chromia we find, complementing our recent work on hematite [Rollmann *et al.*, Phys. Rev. B **69**, 165107 (2004)] that the inclusion of correlation effects leads to an improved description of the structural, electronic, and magnetic properties. In particular, the increased exchange splitting of the *d* band changes the character of the insulating gap from a pure *d-d* Mott-Hubbard type to intermediate between *d-d* and charge-transfer insulator. For both oxides, the strong correlation effects have a dramatic influence on the surface stability: oxygen-terminated surfaces are strongly disfavored because of the increased energetic cost of stabilizing a higher oxidation state of the transition metal close to the surface. The stability of metal-terminated surfaces even under oxidizing conditions agrees with the most recent STM and LEED data. For Cr_2O_3(0001) where detailed experimental information on the surface structure is available, quantitative agreement of the calculated surface relaxations is achieved. Detailed results on the surface electronic structure (valence-band spectra and core-level shifts) and the surface magnetic properties are presented.

I. INTRODUCTION

The corundum-type oxides of iron and chromium, α-Fe_2O_3 and Cr_2O_3, are of great current interest, both from a technological and a fundamental scientific point of view. α-Fe_2O_3 (hematite) is an abundant and important mineral in the Earth's crust, it is an active material in heterogeneous catalysis,[1] and is used as an electrode in photoelectrolysis[2] and in magnetic recording devices. Cr_2O_3 (chromia, mineral name: eskolaite) is also an important catalyst and a major constituent in many ceramics. While Fe_2O_3 is important as a product of the corrosion of Fe surfaces, the formation of a protective Cr_2O_3 overlayer is thought to be an important element in the corrosion resistance of Cr steels. From a theoretical point of view, the main interest in these compounds lies in the role of strong electronic correlations in determining their physical properties—both are antiferromagnetic insulators, but whereas spectroscopic experiments characterize Fe_2O_3 as a charge transfer (CT) insulator, Cr_2O_3 is considered to form a borderline case between a CT and Mott-Hubbard (MH) insulator.[3] It is well known that density-functional theory (DFT) experiences considerable difficulties when trying to achieve a correct description of such strongly correlated materials. However, whereas transition-metal monoxides have received a lot of attention as a paradigmatic case for studying strong electronic correlations (see, e.g., our recent work[4] on NiO and further references therein), it is still current practice to treat the corundum-type transition-metal oxides using DFT.[5] Our recent work[6] on bulk Fe_2O_3 represents one of the first attempts to treat these materials on a post-DFT level.

For bulk hematite and chromia, extended experimental and theoretical studies of the structural, electronic, and mag-

netic properties have been performed.[7–16] Both α-Fe_2O_3 and Cr_2O_3 are antiferromagnetic insulators with band gaps of $\sim$2 eV (Fe_2O_3, Ref. 17) and $\sim$3.4 eV (Cr_2O_3, Refs.18–20), respectively. The Néel temperatures are T_N=955 K (Ref. 21) and T_N=308 K (Ref. 22), respectively. Both materials crystallize in the hexagonal corundum structure (space group $R\bar{3}c$), with six formula units in the bulk unit cell (Ref. 23). The atoms are stacked in the order $\cdots$TM-TM-$O_3\cdots$ along the [0001] axis. Each TM atom has a distorted octahedral environment of six oxygen nearest neighbors. The intralayer nearest neighbor (NN) TM-TM distance is shorter than the interlayer TM-TM NN distance. The antiferromagnetic order of the TM layers along [0001] is ++−− for Fe_2O_3 and +−+− Cr_2O_3. Both oxides experience strong correlation amongst their localized 3*d* electrons. *Ab initio* density functional studies of bulk α-Fe_2O_3 (Refs. 6, 10, and 11) have shown that these correlation effects cannot be appropriately treated within the local spin-density approximation (LSDA), even with the spin-polarized generalized-gradient approximation (SGGA). The calculations show too small or even no band gaps, too small magnetic moments, and also incorrect positions of the 3*d* orbitals in relation to the oxygen states, characterizing Fe_2O_3 as a *d-d* Mott-Hubbard insulator, whereas the spectroscopic evidence argues in favor of a charge-transfer insulator.[3,24,25] Hartree-Fock studies,[12] on the other hand, lead to a gross overestimation of the energy gap and far too small bandwidths. For Cr_2O_3 photoemission studies of both valence states and core levels[3,16,26,27] and inverse photoemission experiments [27] support a classification as an intermediate-type insulator between charge-transfer and Mott-Hubbard insulators. While this characterization is supported by the Hartree-Fock study of Catti *et al.*,[12] the calculated energy gap of about 15 eV is again far too large. For

chromia a DFT study by Dobin *et al.*[15] using the LSDA predicts a too small gap of only ~ 1.5 eV. Wolter *et al.*[28] also used the LSDA to determine the ground state of Cr_2O_3, but find a ferromagnetic state to be lower in energy than the antiferromagnetic phase, in contradiction to experiment. For TM monoxides it has been shown that the problems inherent in DFT studies can be largely overcome by adopting a DFT$+U$ approach, where the effects of strong intra-atomic electronic correlations are modeled by adding an on-site Coulomb repulsion U to the DFT Hamiltonian.[4,29,30,33] Very recently we have shown that the DFT$+U$ approach also leads to a satisfactory description of the structural, electronic, and magnetic properties of hematite.[6]

The (0001) surfaces of α-Fe_2O_3 and Cr_2O_3 have been subject to intensive studies—experimentally as well as theoretically—due to their importance as catalysts. Experimental studies have been conducted to investigate the heterogeneous surface structures in varying oxygen atmospheres with STM and LEED measurements as well as HREELS and core-level measurements (XPS) for the clean surfaces and surfaces covered with adsorbed molecules for Fe_2O_3 (Ref.34–38) and Cr_2O_3 (Ref. 28 and 39–45) to elucidate the surface chemical reactivity. However, a comprehensive understanding of the surface properties of hematite and also of chromia is still lacking. The reason is that the preparation of clean surfaces with well-defined structures and stoichiometries can require high oxygen pressures which are hard to reconcile with experiments in ultrahigh vacuum environments. Furthermore, the use of photoelectron spectroscopies (PES) and of scanning tunneling microscopy is difficult because of the insulating character of the materials. For Cr_2O_3, a low-energy electron diffraction (LEED) analysis of the surface structure has been performed,[42] demonstrating a 60% inward relaxation for the first Cr-O_3 interlayer distance on a Cr-terminated surface, and also large relaxations of the distances between the deeper layers extending as deep as to the fourth subsurface layer. Maurice *et al.*[45] also concluded on the basis of a combined XPS, LEED, and STM investigation that the (0001) surface of thin Cr_2O_3 films formed on $Cr(110)$ substrates are Cr terminated.

For Fe_2O_3 no LEED analysis exists so far. Computer simulations of the structure of Fe_2O_3 surfaces have shown that no comparable surface relaxation is predicted by calculations based on static ions,[46] whereas semiempirical calculations based on polarizable ions[47,48] and *ab initio* DFT calculations[5] predict large inward relaxations in surprisingly close agreement with those measured for the Cr_2O_3 surface. The *ab initio* calculations of Wang *et al.*[5] predict that the Fe-terminated surface of Fe_2O_3 is stable under low oxygen pressures, at an increased chemical potential of oxygen, a transition to an oxygen-terminated surface structure is predicted. This oxygen terminated surface should show only a minimal relaxation of the first O_3-Fe interlayer distance, but an even larger contraction of the Fe-O_3 distance between the subsurface layers. STM experiments on Fe_2O_3 surfaces produced by the oxidation of thick Fe_3O_4 films grown on $Pt(111)$ accompanying the *ab-initio* calculations have demonstrated the coexistence of two different surface terminations which have been attributed to the Fe- and the O_3-terminated surfaces predicted by the DFT calculations.

However, this interpretation has not been confirmed by the most recent STM study of Chambers and Yi[49] on hematite films produced by oxygen-plasma assisted molecular beam epitaxy (i.e., under strongly oxidizing conditions) which found only an Fe-terminated surface.

For (0001)-Cr_2O_3 where a direct confrontation between theory and experiment would be possible, the embedded-cluster HF calculations[39,40] for the Cr-terminated surface have restricted relaxation to the Cr-O_3 and O_3-Cr interlayer distances at the surface. Reasonable agreement for the strong inward relaxation of the top Cr layer was reported, but the strong contraction of the Cr-Cr distances in the subsurface layer was not examined. Very recently Wang and Smith[50] reported an *ab initio* density functional study of the Cr_2O_3 surface using the GGA and the same computational approach as used by Scheffler *et al.*[5] for the hematite surface. It was concluded that depending on oxygen chemical potential and temperature, the surface can be Cr terminated, chromyl terminated, or O terminated. However, no information on the surface relaxation and on the magnetic state is given in this short paper.

It is expected that different surface terminations will also lead to significant differences in the electronic and magnetic properties of the surfaces, but so far no indications for the existence of different terminations could be found in the spectroscopic data. It is also a bit puzzling—and eventually only coincidental—that Cr_2O_3 which has been described as an intermediate CT/MH insulator and the CT-insulator Fe_2O_3 should show such similarity in their surface relaxations. Surface relaxations and reconstructions are always associated with charge-redistributions between the occupied and empty electronic surface states. DFT calculations are known to substantially underestimate the energy gap. Hence the question arises whether the prediction of the coexistence of two different surface terminations will also hold if the DFT approach is corrected for the missing intra-atomic correlations. For the $NiO(100)$ surface we have shown[4] that the DFT$+U$ approach leads to significantly different predictions of the surface chemical reactivity compared to the DFT: only within the DFT$+U$ the adsorption geometry and energetics of CO and NO adsorbed on $NiO(100)$ is correctly described.

The present work is devoted to a DFT$+U$ investigation of the (0001) surfaces of α-Fe_2O_3 and Cr_2O_3. The paper is organized as follows. Section II reviews very briefly the underlying theory and the computational details of the calculations, it also presents the fundamental thermodynamic aspects of surface stability under varying atmospheres. Section III summarizes the results of DFT$+U$ calculations for bulk Cr_2O_3. Section IV presents the results for the $Fe_2O_3(0001)$ surface and Sec. V follows up with the results for the $Cr_2O_3(0001)$ surface. The paper is finished with concluding remarks in Sec. VI.

II. METHODS

A. Computational details

The present calculations have been performed with the Vienna *ab initio* simulation package VASP,[51–55] a first-

principles plane-wave code based on spin-polarized density functional theory (DFT). Exchange correlation was treated with an LDA functional by Perdew and Zunger[56] and generalized gradient corrections (GGA) added in the form of the Perdew-Wang[57] functional. The spin interpolation of Vosko *et al.*[58] was used. The electron-ion interaction was described with the projector augmented wave (PAW) method[59] in the implementation of Kresse and Joubert.[60] The Kohn-Sham equations were solved via iterative matrix diagonalization based on the minimization of the norm of the residual vector to each eigenstate and optimized charge- and spin-mixing routines.[61–63]

The Brillouin zone integration is performed using Monkhorst-Pack grids.[64] k-point grids with a $4 \times 4 \times 1$ mesh for relaxations and a $8 \times 8 \times 1$ mesh for the calculation of densities of states (DOS) where used. For the force calculations used to relax the lattice parameters and internal coordinates, a Gaussian-smearing approach with $\sigma = 0.1$ eV was used, and DOS calculations were performed with the linear tetrahedron method. The plane-wave energy cutoff was fixed to 350 eV for both Fe_2O_3 and Cr_2O_3. The optimization of the surface structure has been performed using quasi-Newton and conjugate gradient algorithms.

Partial electronic densities of state were calculated by projecting the plane-wave components of the electronic eigenstates onto their spherical harmonic components within atomic spheres.[65] Here the angular-momentum decomposed components are defined with respect to a Cartesian coordinate system with one of the axes perpendicular to the surface.

Core-level binding energies have been calculated, including final state effects, using a modified PAW method.[66] A single core electron is excited from the core to the valence by generating a "core-excited" PAW potential. Screening by the core electrons is not taken into account (i.e., the other core electrons were kept frozen in the configuration for which the PAW potential was generated). Screening by the valence electrons is included. A careful comparison with the results of full-potential calculations has demonstrated the reliability of this approach.

To correct for the strong electronic correlation, the DFT $+U$ method in the form proposed by Liechtenstein and Dudarev *et al.*,[29,30,32,33] and implemented in a PAW approach by Bengone *et al.*[31] was used. For the implementation within VASP and a more detailed description of the GGA$+U$ method, the reader is referred to Ref. 67. Here we only emphasize that in order to achieve a reasonable overall agreement with experiment, it is necessary to combine the Hubbard-like description of the on-site correlations with DFT calculations at the level of a spin-polarized GGA, we refer to this approach as GGA$+U$. At the LDA$+U$ level, different values of the on-site potential U are necessary for a correct description of the crystal structure and of the electronic properties: usually a correct atomic volume is achieved only with a very large value of U, leading to a substantial overestimation of the energy gap—for a detailed comparison of the LDA$+U$ and GGA$+U$ approaches, see our earlier work on transition-metal sulfides[67] and on bulk and surface of nickel monoxide.[4] However, it has to be admitted that due to the empirical character of the Hubbard

correction, the application of the DFT$+U$ approach to the question of surface phase stability is subject to some uncertainty: it is conceivable that the optimal value of the on-site potential determined for the bulk does not apply at the surface. Similarly, a comparison of the energies of phases with different stoichiometries is not straightforward within DFT $+U$. We shall return to this question below.

B. Surface models

The polar (0001) surface has been modeled by symmetric slabs containing six TM_2O_3 layers for the oxygen-terminated surfaces and a 1×1 periodicity in the surface. The use of symmetric slabs cancels out dipole moments, which can occur in nonsymmetric slabs. The lateral dimensions of the surface cell were kept fixed, but the ions in the first five atomic layers (top and bottom) were free to relax. Figure 1 (I) shows the structure of an oxygen-terminated surface. Altogether for both materials, we have investigated five different terminations (three oxygen terminations and two TM terminations). The surface terminations based on cleaved bulklike structures are $\cdots$-$O_3TM_2O_3$ (model I), $\cdots$-$TM_2O_3TM_2$ (II) and $\cdots$-TM_2O_3TM (where half of the TM atoms have been eliminated from the top layer—model III). More sophisticated terminations are $\cdots$-TM_2O_3TMO, which ends with a layer of ferryl or chromyl groups, and $\cdots$-$TMO_3TM_3O_3$, where a TM atom jumps from the second TM layer to the first TM layer [see Fig. 1 (II)]. These two surface terminations have already been tested for the isostructural V_2O_3(0001) surfaces by Kresse *et al.*[68] and proved to be useful for the understanding of the transition from vanadium-terminated to oxygen-terminated surfaces in the phase diagram. For the oxygen-terminated $\cdots$-$TMO_3TM_3O_3$ surface where half of the metal atoms from the second metal layer have migrated to the near-surface layer all octahedral positions in this layer are occupied (model IV). The ferryl, respectively, chromyl-terminated $\cdots$-TM_2O_3TMO surface represents model V.

It is important to emphasize that the surface terminations I–IV differ in the charges exposed at the free surface. In particular, the oxygen-terminated surfaces I and IV represent an excess of negative charges at the surface which is only partially compensated in model V ($\cdots$-$TMO_3TM_3O_3$) by moving metal atoms from a deeper layer to the surface, filling the vacant octahedral position. Similarly, the TM-terminated surface II and III expose positive charges at the surface, and the reduced occupancy of the TM-surface layer in model III ($\cdots$-TM_2O_3TM) is a possibility to reduce surface charges.

The slab calculations have been started with the same magnetic ordering as for the bulk calculations, but spin reorientations are admitted during the electronic self-consistency cycle. Similar initial settings were also used for Fe_2O_3 slabs in Ref. 5 and the spin-alignment in the bulk is strictly along the c axis.

C. Thermodynamical aspects

The determination of surface stability under a varying partial pressure of oxygen is based on a few simple thermo-
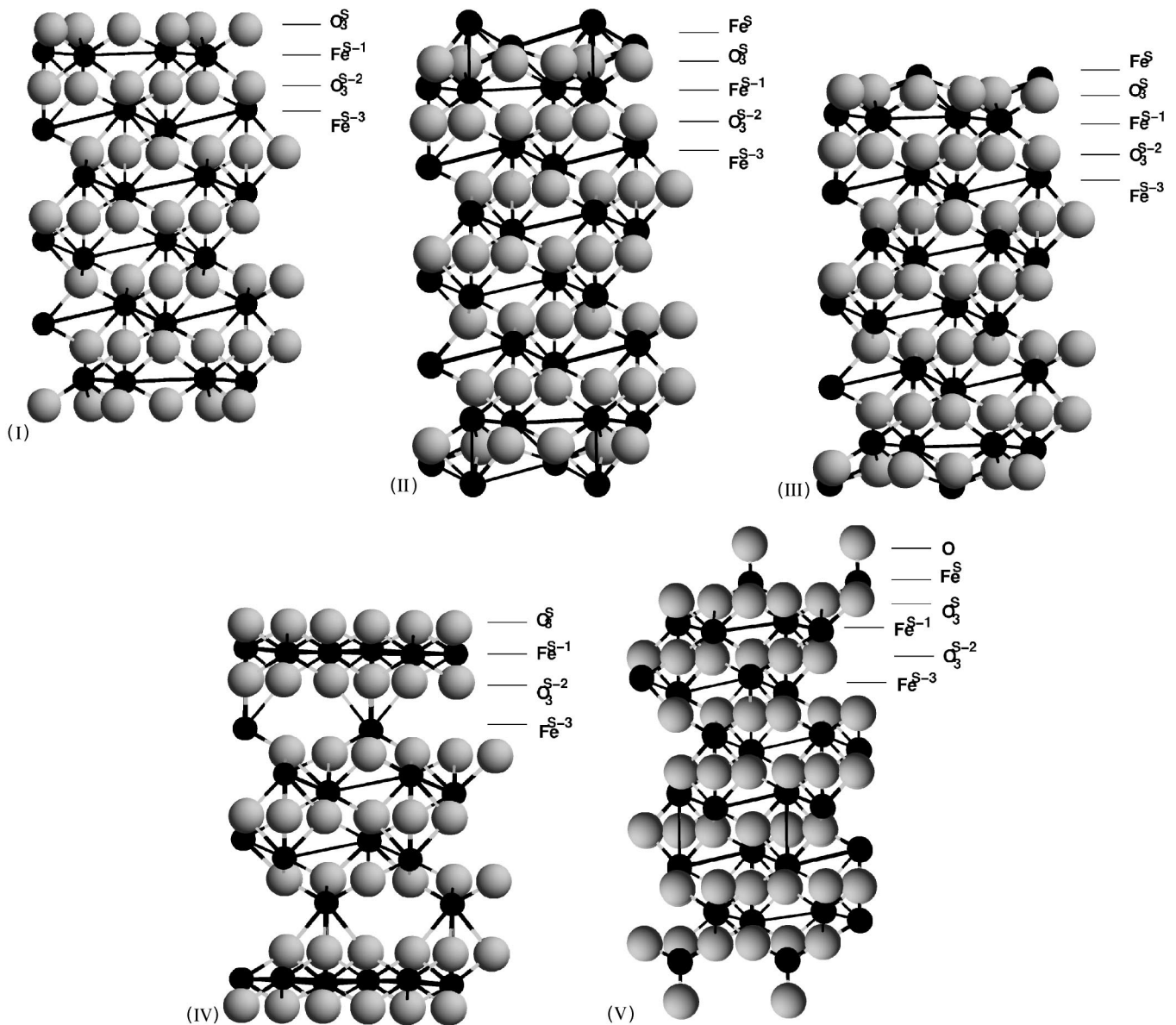
FIG. 1. Slab model of the (relaxed). $\cdots$-TM$_2$O$_3$ terminated surface with bulklike geometry (I)—large grey balls represent oxygen atoms with small black balls TM atoms. $\cdots$-TM$_2$O$_3$ (bulk)-TM$_2$ transition-metal terminated surface with a bulklike geometry may be created by adding a full TM layer to this slab (II). $\cdots$-TM$_2$O$_3$ (bulk)-TM transition-metal terminated surface is created by eliminating half of the TM atoms from the surface layer (III). (IV) Slab representing the reconstructed $\cdots$-TMO$_3$TM$_3$O$_3$ terminated surface. This structure is created by the migration of a TM atom from a deeper layer to the subsurface TM layer. (V) Slab representing a ferryl/chromyl terminated surface.

dynamic arguments. Here we follow the approach developed by Scheffler *et al.*[69] For a surface in thermal equilibrium with the oxygen gas, the important quantity is the surface energy

$$\gamma = [G(T,p,\{n_x\}) - \sum_x n_x \mu_x(T,p_x)]/A, \tag{1}$$

which is given by the Gibbs free energy G, the number n_x of particles of type $x[x=\text{Cr}(\text{Fe}),\text{O}]$ in the solid and the chemical potentials μ_x at temperature T and pressure p (p_x is the partial pressure), and the total surface area A. The Gibbs free energies can be approximated by the internal energies $E(T=0,p=0,\{n_x\})$ from DFT(DFT+U) calculations. For TM$_2$O$_3$

compounds thermal equilibrium between surface and bulk requires that

$$2\mu_{\text{TM}} + 3\mu_{\text{O}} = E_{\text{TM}_2\text{O}_3}, \tag{2}$$

where $E_{\text{TM}_2\text{O}_3}$ is the DFT energy of bulk TM$_2$O$_3$. This relation can be used to eliminate the dependence of the surface energy on the chemical potential of the transition metal. In this approximation and imposing equilibrium, the surface energy γ can be written as

$$\gamma = [E\{n_x\} - n_{\text{TM}}E_{\text{TM}_2\text{O}_3}/2 - (n_\text{O} - 3/2n_{\text{TM}})\mu_\text{O}]/A. \tag{3}$$

This surface energy depends on the total energy of the slab, the slab stoichiometry, and the oxygen chemical poten-

TABLE I. Lattice constants a and c, axial ratio c/a, TM-TM distances TM-TM(A) and TM-TM(B), magnetic moments μ, bulk modulus B, and band gap E_g of antiferromagnetic corundum-type α-Fe$_2$O$_3$ and Cr$_2$O$_3$. For the GGA+U calculations the value U=5 eV and J=1 eV have been used for the on-site Coulomb-repulsion and the exchange integral, respectively.

	a[Å]	c[Å]	c/a	Fe-Fe(A) [Å]	Fe-Fe(B) [Å]	$\mu[\mu_B$/atom]	B[GPa]	E_g[eV]
				α-Fe$_2$O$_3$				
GGA	5.007	13.829	2.772	2.929	3.998	3.45	173.0	0.5
GGA+U	5.067	13.882	2.739	2.896	4.044	4.11	191.9	2.0
Exp.[a]	5.029	13.730	2.730	2.883	3.982	4.6–4.9[c]		
Exp.[b]	5.035	13.747	2.730	2.896	3.977		178,225	2.0
	a[Å]	c[Å]	c/a	Cr-Cr(A) [Å]	Cr-Cr(B) [Å]	$\mu[\mu_B$/atom]	B[GPa]	E_g[eV]
				α-Cr$_2$O$_3$				
GGA	4.941	13.829	2.798	2.642	4.271	2.68	204.3	1.2
GGA+U[c]	5.073	13.839	2.727	2.723	4.196	3.01	229.5	2.6
Exp.[d]	4.951	13.566	2.740	2.623	4.085	3.8	222,238	3.4

[a]After Pauling and Hendricks (Ref. 23).
[b]Structural data after Finger and Hazen (Ref. 70), bulk modulus from Sato and Akimoto (Ref. 71), (the two different values correspond to fits of the equation of state over different pressure ranges), and energy gap according to Ref. 17.
[c]After Coey and Sawatzky (Ref. 72) and Kren *et al.* (Ref. 73).
[d]Structural data after Finger and Hazen (Ref. 70) and energy gap according to Refs. 18–20.

tial. To determine the surface stability in an oxygen atmosphere, the surface energy calculated for different surface terminations (i.e., different slab stoichiometries) is plotted against the oxygen chemical potential. The termination with the lowest energy at a given chemical potential is the stable surface at this oxygen partial pressure.

The chemical potential μ_O can vary only within a limited range. At the lower limit, reduction of the oxide from Fe$_2$O$_3$ (hematite) to Fe$_3$O$_4$ (magnetite) and further to FeO (wustite) and to metallic Fe, or from Cr$_2$O$_3$ to metallic Cr will set in. At at the upper limit, oxygen starts to condensate on the surface of hematite and Cr$_2$O$_3$ is oxidized to CrO$_2$. The limiting values for μ_O are therefore given for hematite surfaces by

$$3G_{\text{Fe}_2\text{O}_3}^{\text{bulk}} - 2G_{\text{Fe}_3\text{O}_4}^{\text{bulk}} \leq \mu_O \leq 1/2\mu_{\text{O}_2} \qquad (4)$$

and for chromia by

$$\frac{1}{3}(G_{\text{Cr}_2\text{O}_3}^{\text{bulk}} - 2G_{\text{Cr}}^{\text{bulk}}) \leq \mu_O \leq 2G_{\text{CrO}_2}^{\text{bulk}} - G_{\text{Cr}_2\text{O}_3}^{\text{bulk}}. \qquad (5)$$

This limit explains the range with negative surface energies in the phase diagram for Cr$_2$O$_3$(0001), where Cr$_2$O$_3$ is oxidized to CrO$_2$. However, at this place a cautionary remark concerning DFT+U calculation is necessary: while in DFT calculations, the comparison of total energies of phases of different stoichiometry is unproblematic, in DFT+U calculations the possibility of a variation of the on-site Coulomb repulsion with stoichiometry introduces some uncertainty. As a detailed study of magnetite is outside the scope of the present work, the lower limit of the oxygen chemical potential is determined for both oxides relative to the pure metal, using the GGA and the GGA+U (with the same value of U as for the oxide).

III. STRUCTURE, ELECTRONIC, AND MAGNETIC PROPERTIES OF CR$_2$O$_3$

The calculated structural parameters for both oxides are summarized in Table I. In our work on bulk hematite[6] we have determined a value of U=5 eV as leading to the optimal agreement between theory and experiment for a wide range of physical properties. A similar investigation has also been performed for chromia: ground-state properties have been determined for Coulomb parameters ranging from $U-J$=0 eV (GGA limit) up to $U-J$=8 eV, together with a constant exchange parameter J=1 eV. Figure 2 shows that equilibrium volume, band gap, and magnetic moment increase with increasing strength of the on-site correlations. The magnetic moment and the band gap remain below the experimental values, whereas the equilibrium atomic volume is overestimated slightly compared to experiment even in the GGA limit. As for hematite, a value of U=5 eV leads to an acceptable compromise between the structural and the electronic properties. The apparent discrepancy of the calculated magnetic moment is probably not so serious as the experimental estimate is strongly based on a purely ionic picture of the compound—an assumption to be tested against the electronic structure. One should also note that the theoretical gap listed in Table I measures the distances between the band edges, whereas the experimental gap measures the optical adsorption peak (see also below).

Altogether, the GGA+U leads to a significantly improved description of the structural, magnetic, and electronic properties of both materials compared to the GGA. Concerning the crystal structure we note that along the hexagonal c axis, the corundum structure has an alternating series of closed-packed oxygen layers followed by layers with two TM atoms occupying two thirds of the octahedral sites formed by the hexagonal close-packed array of the oxygen atoms. The oxygens are aligned such that each TM atom has a slightly dis-
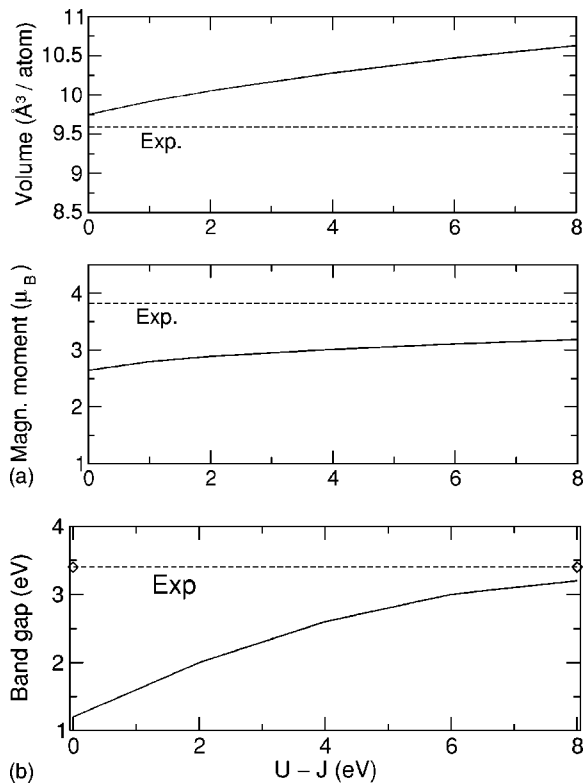
FIG. 2. Atomic volume, magnetic moment, and band gap for Cr_2O_3 plotted against $U-J$. $U-J=0$ represents the GGA limit.

torted octahedral environment. Along the hexagonal axis short (A) and long (B) distances between the TM layers alternate (see Fig. 1 in Ref. 6). The GGA+U leads to a better agreement of the ratio between short and long TM-TM distances and hence to a more realistic local geometry. For the antiferromagnetic structure, different stacking sequences of spin-up and spin-down moments (++−−, +−+−, and +−−+) are possible. For Fe_2O_3 the ++−− state with opposite moments on Fe atoms with short (A) distances was found to

represent the magnetic ground state, in agreement with experiment. In contrast, for Cr_2O_3 the spin orientation in the TM layers stacked along the c axis +−+−, hence the coupling between neighboring Cr layers is antiferromagnetic. Within the GGA the +−+− stacking sequence is lower in energy by 20.8 meV (all energy differences are per Cr atom) compared to the +−−+ stacking, by 46.6 meV compared to ferromagnetic ordering, and by 47.7 meV relative to ++−− stacking, in agreement with experimental observation. Strong electronic correlations tend to reduce the magnetic energy differences. The +−+− phase still represents the magnetic ground state, but it is lower in energy by only 6.3 meV compared to the ferromagnetic phase, and by 8.4 and 19.0 meV compared to the antiferromagnetic +−−+ and ++ −− phases, respectively.

Figure 3 shows the O-$2p$ and the Cr-e_g and t_{2g} derived electronic densities of state as calculated in the GGA and in the GGA+U.

The structure of the d band corresponds to the splitting of the Fe-d states in the nearly octahedral ligand field of the surrounding O atoms into nonbonding t_{2g} states and bonding and antibonding e_g states. One must say that because the CrO_6 octahedra in the corundum structure are not aligned with the c axis, the decomposition we have adopted (see Sec. II A) does not exactly correspond to the irreducible representations of the octahedral point group. However, we find this much simpler approach to be sufficient for analyzing the electronic structure. This applies particularly to the analysis of the near-surface DOS where the relaxation leads to an appreciable distortion of the coordination octahedra.

In the GGA, the Cr-O hybridization is very weak, the energy gap of about 1.2 eV is between the highest occupied majority valence-band state of Cr-t_{2g} character, and the lowest conduction-band state of mixed majority Cr-e_g/minority Cr-t_{2g} character, classifying chromia as a d-d Mott-Hubbard insulator.

The on-site Coulomb interaction shifts the occupied Cr-d states to higher binding energies and leads to an increased Cr-$3d$-O-$2p$ hybridization. The energy gap of about 2.6 eV
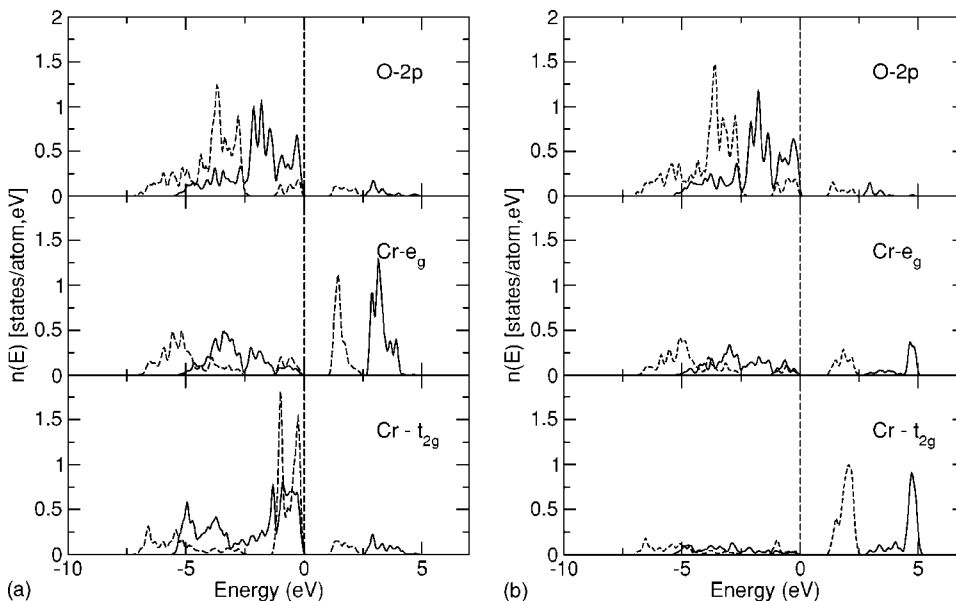

FIG. 3. Density of states of bulk Cr_2O_3 calculated with GGA (dashed line) and GGA+U (full line).

(band edges) is now between a highest valence-band state of strongly mixed Cr-t_{2g}-O-$2p$ character and a lowest conduction band state of Cr-e_g character, in accordance with the experimental classification of chromia as an intermediate CT-MH insulator.[3,16,26,27] The electronic structure calculated in the GGA+U is in very good agreement with the combined PES and inverse PES experiments of Zimmermann *et al.*[16] Taking the energy difference between the valence- and conduction-band peaks leads to a gap of about 3 eV (theory) compared to 3.4 eV (PES and inverse PES). The narrow and asymmetric shape of the empty Cr-e_g band agrees well with inverse PES spectrum, the analysis of the partial photoexcitation spectra in the basis of the energy-dependent photoionization cross sections confirms the strong overlap of the Cr-$3d$ and O-$2p$ derived features over the entire valence-band region.[16] Hence we can conclude that for Cr_2O_3, as already found for Fe_2O_3, a GGA+U description leads to a significantly improved description of the physical properties. In particular we note the profound modification of the "frontier orbitals" (the highest occupied valence states)—this will evidently be an important element in determining surface stability and chemical reactivity.

IV. Fe₂O₃(0001) SURFACES

A. Phase stability

Phase diagrams for Fe_2O_3(0001) surfaces have been calculated within the GGA and the GGA+U approaches. Theoretical studies[6] of bulk Fe_2O_3 with GGA+U have shown that an on-site Coulomb interaction of $U=5$ eV together with an exchange parameter of $J\sim 1$ eV leads to an accurate description of the structural, electronic, and magnetic properties. We have chosen the same values for the surface calculations. The variation of the surface energy with the chemical potential of oxygen from the GGA calculations [Fig. 4(a)] leads to a phase diagram very similar to that published by Scheffler *et al.*[5] In the oxygen-poor range up to a chemical potential of $\mu_O=-1.3$ eV, the surface is iron terminated ($\cdots$-Fe_2O_3Fe—model III) with a bulklike structure (but large changes in the interlayer distances and 50% vacancies in the top Fe layer). An Fe-terminated bulklike surface with a full Fe coverage in the top layer ($\cdots$-$Fe_2O_3Fe_2$—model II) is strongly disfavored under oxidizing conditions and becomes stable only outside the lower limiting value of the chemical potential indicating the instability of the oxide surface against the formation of Fe clusters (the possibility of the formation of a Fe_3O_4 overlayer is not considered here, this would push the limiting value of the chemical potential to higher values). Under a more oxygen rich atmosphere, the surface becomes oxygen terminated. In contrast to Ref. 5, the transition is not abrupt, but there is a transition range of ~ 0.3 eV, where a ferryl-terminated ($\cdots$-Fe_2O_3FeO—model V) surface becomes stable. This surface structure was not considered in the previous DFT study. Another surprising result is that the stable oxygen-terminated surface is $\cdots$-$FeO_3Fe_3O_3$ (i.e., all octahedral sites are occupied in the uppermost Fe layer, while the next Fe layer is depleted—model IV) rather than the simple bulk-terminated $\cdots$-$Fe_2O_3Fe_2O_3$ (model I) surface. It seems that the missing
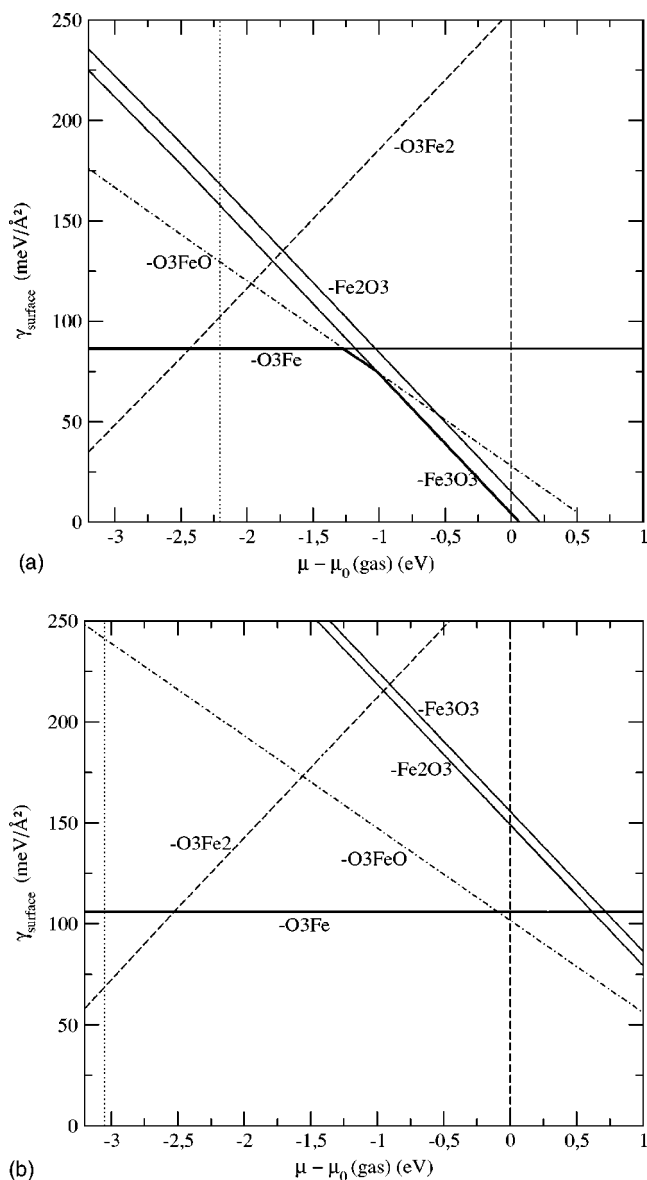

FIG. 4. (a) GGA derived surface energies of the different terminations plotted against oxygen chemical potentials. (b) GGA+U derived surface energies plotted against oxygen chemical potentials. The vertical lines mark the allowed range of the chemical potential, as limited from above by the condensation of molecular oxygen at the reduced and from below by the reduction of Fe_2O_3 to Fe (see text).

iron layer on top of the surface has to be compensated by taking an additional iron atom into the first iron sublayer, since the iron terminated surface is stable under vacuum conditions. A similar reconstructed $\cdots$-$VO_3V_3O_3$ has been found by Kresse *et al.*[68] on the V_2O_3(0001) surface, but it has not been considered so far for hematite. Altogether we find that both under oxidizing and reducing conditions surface terminations leading to reduced surface charges are prefered: $\cdots$-$FeO_3Fe_3O_3$ (IV) over $\cdots$-$Fe_2O_3Fe_2O_3$ (I) at high partial pressures of oxygen, $\cdots$-Fe_2O_3Fe (model III) over $\cdots$-$Fe_2O_3Fe_2$ (model II) under reducing conditions.

Experimental STM results[5] present evidence for the coexistence of two different surface terminations under oxygen-

TABLE II. Surface relaxation for the four relevant terminations of the $Fe_2O_3(0001)$ surface. The relaxations of the first three ML and the first two interlayer Fe-Fe distances are given in percent of the bulk interlayer Fe-O and Fe-Fe distances. Both distances are projected onto the hexagonal c axis. The bulk interlayer Fe-O distance is 0.85 Å and the interlayer Fe-Fe distance is 0.62 Å for GGA/GGA+U. For comparison the FLAPW results obtained by the GGA are included. For the nomenclature, see Fig. 1.

| | ···-$Fe_2O_3FeO_3$ (V) | | ···-Fe_2O_3Fe(III) | | | ···-$Fe_2O_3Fe_2O_3$ (I) | | | ···-$FeO_3Fe_3O_3$(IV) | |
	GGA	GGA+U	GGA	GGA+U	FLAPW[a]	GGA	GGA+U	FLAPW[a]	GGA	GGA+U
O-Fe^S	−15	−16								
Fe^S-O_3^S	−16	−18	−53	−57	−57					
O_3^S-Fe^{S-1}	1.6	1.0	22	9.6	7	−4.9	−7.4	−1	−6.7	−2.3
Fe-Fe^{S-1}	−40	−34	−31	−40	−33	−71	−53	−79	−73	−63
Fe^{S-1}-O_3^{S-3}	16	18	34	17	15	23	37	37	8.7	15.4
O_3^{S-2}-Fe^{S-3}	−2.5	−1.1	2.5	3.5	5	−5.7	−6.0	−6	−5.3	9.0
Fe-Fe^{S-3}	9.5	1.9	−9.8	−4.4	−3	17	16	16		

[a]After Scheffler *et al.* (Ref. 5).

rich conditions [a 100 Å film of Fe_3O_4 grown on Pt(111) was oxidized to Fe_2O_3 by high-temperature annealing under an excess oxygen pressure of $\sim 10^{-3}$ Torr]. For both types of surfaces, atomically resolved STM images reveal a hexagonal symmetry with a periodicity compatible with the interatomic distance within the Fe layers of the corundum structure. The step height at the boundary is about 1 Å i.e., substantially lower than the distance of 2.28 Å between two equivalent surface terminations of α-Fe_2O_3. The two terminations were therefore associated with the iron-terminated surface stable under oxygen-poor environments and an oxygen-terminated surface. However, a more detailed experimental characterization could not be given. Another STM study[37] reports three different surface terminations. Upon high-temperature annealing (i.e., under reductive conditions) an epitaxial Fe_3O_4(111) layer is formed, with two coexisting surface terminations consistent with previous studies of the (111) surface of magnetite.[74,75] At higher oxygen pressures, a long-period superstructure consisting of a regular array of Fe_2O_3(0001) and $Fe_{1-x}O$(111) domains was reported. The periodicities within these domains are 5 and 3 Å, respectively, but the STM features could not be uniquely assigned to Fe or O atoms. In the most recent STM study of the Fe_2O_3(0001) surface,[49] Fe_2O_3 films prepared by oxygen-plasma assisted molecular beam epitaxy have been investigated. After stopping the growth, the specimen was allowed to cool to room temperature while being exposed to the same oxygen plasma used during the film preparation. Despite the highly oxidizing conditions used to end the film growth, the surface was found to be iron terminated, in contrast to the interpretation of the earlier STM experiments.

The surface energies resulting from GGA+U calculations [Fig. 4(b)] demonstrate a dramatic change of the relative stabilities of the different surface terminations relative to the GGA. Whereas the iron-terminated surface shows a similar surface energy, the energies of oxygen-terminated surfaces increase strongly. As a consequence both the bulk-terminated ···-$Fe_2O_3Fe_2O_3$ (model I) and the reconstructed ···-$FeO_3Fe_3O_3$ (model IV) oxygen-terminated surfaces are predicted to be unstable over the entire admissible range of the chemical potential of oxygen. Their relative stability is

reversed relative to the GGA case, demonstrating that a local balance of charges is not as important as in the absence of strong correlations. Under strongly reducing conditions the Fe-terminated ···-$Fe_2O_3Fe_2$ (model II) surface without Fe surface vacancies is found to be stable. However, under reducing conditions, the ···-$Fe_2O_3Fe_2$ (model II) surface competes with the formation of an Fe_3O_4 overlayer, which is not considered here. The iron-terminated surface is stable up to a chemical potential of $\mu_O \sim -0.2$ eV. The ferryl-terminated surface is stable only in the oxygen-rich limit of the phase diagram. Hence the question concerning the nature of the two coexisting surface terminations reported on the basis of the STM work[5] remains open. The STM study also revealed a much stronger corrugation of the "O-terminated" than for the Fe-terminated surface regions. This observation agrees with the geometric structure of the ferryl-terminated surface. The more recent STM study performed under largely oxidizing conditions provides, however, does not support coexisting surface terminations. Thus, altogether GGA+U indicate Fe termination to be stable over a wide range of O pressures, and only a marginal stability of a ferryl-terminated surface, is found to be in fair agreement with experiment.

The dramatic change in the phase stabilities arising from the strong electronic correlation effects is a consequence of the profound modification of the electronic structure. The on-site Coulomb-repulsion shifts the occupied Fe-d band to higher binding energies. The formation of a terminating oxygen overlayer leads to an increased oxidation state of the underlying Fe atoms and a shift of the near-surface Fe-d states to lower binding energies. The energetic cost is higher in the GGA+U as, due to the on-site correlations, the Fe-d states are lowered in energy. Details of the surface electronic structure for different terminations are discussed below.

B. Surface structure

The structural details of the relaxed slabs for the five different surface terminations are given in Table II. Overall, the results of GGA and GGA+U calculations are similar. The comparison with the FLAPW results of Ref. 5 shows good agreement for the Fe-terminated ···Fe_2O_3Fe (model III) and

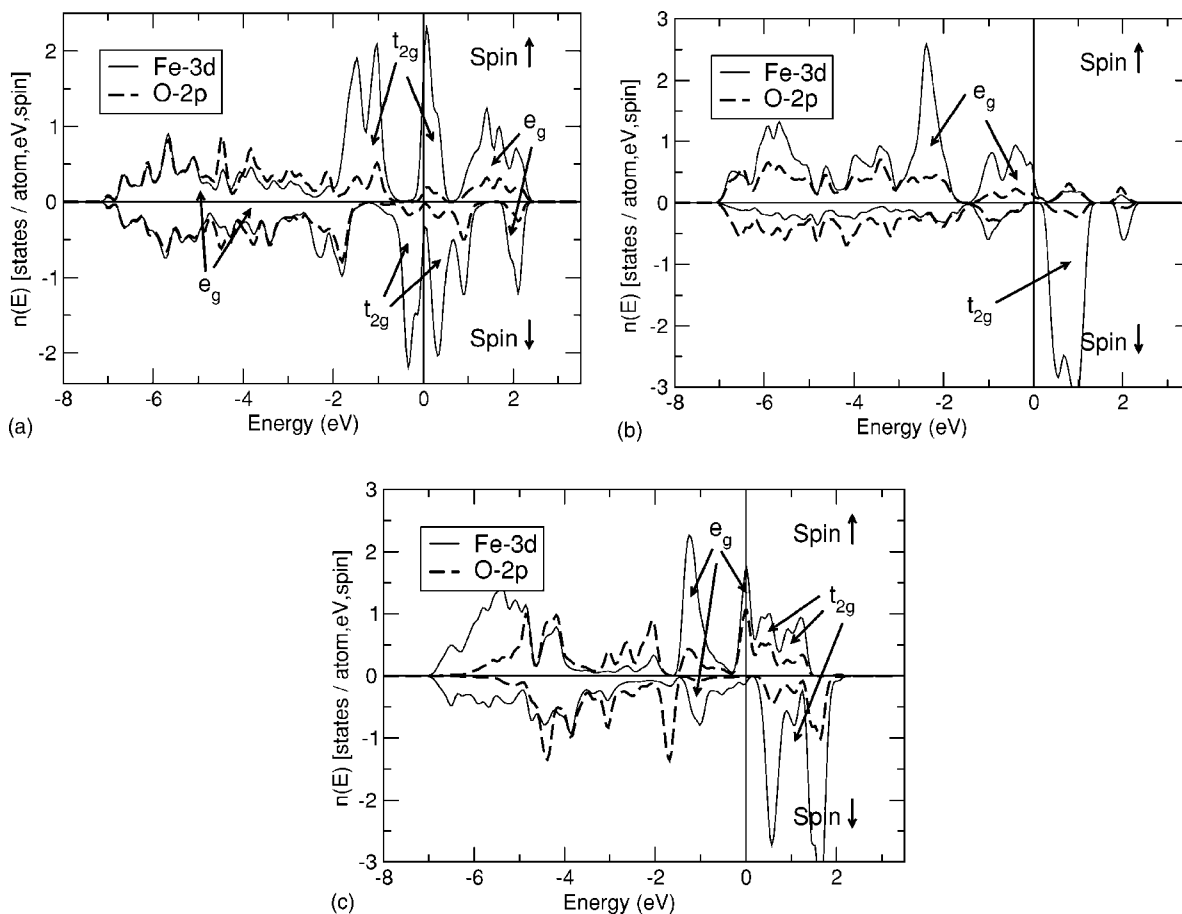FIG. 5. Electronic densities of states of near-surface layers (printed boldface) of the $\cdots$-FeO$_3$Fe$_3$O$_3$ terminated (a), the $\cdots$-Fe$_2$O$_3$Fe terminated (b), and the $\cdots$-Fe$_2$O$_3$FeO terminated (c) Fe$_2$O$_3$-(0001) surfaces from GGA calculations.

the oxygen-terminated $\cdots$-Fe$_2$O$_3$Fe$_2$O$_3$ (model I) surface with bulklike order (which we find, however, to be less stable than the reconstructed $\cdots$-FeO$_3$Fe$_3$O$_3$ surface of model IV). It is remarkable that the consideration of the on-site Coulomb correlation has only a marginal influence on the interlayer relaxation. The comparison with force-field calculations[46,47] for the iron-terminated surface also shows reasonable agreement, as long as the polarizability of the ions is taken into account. We take the small difference between GGA, GGA+U, and force-field calculations as an indication that the interlayer relaxations are determined mainly by a tendency to reduce the large dipole moments of the surface layer of these polar surfaces and not so much by details of the surface electronic structure.

For the Fe-terminated surface, the largest relaxation effects are the reduction of the Fe-O distance between the two top layers (which is essentially an electrostatic effect characteristic for this polar surface) and the flattening of the Fe bilayer (which is rather a consequence of the compression of the top Fe-O layer). The predicted interlayer relaxations are in almost quantitative agreement with the theoretical results for Cr$_2$O$_3$ (see below) and also with the LEED data for this chromia surface—again this supports the argument that the relaxation is dominated by electrostatic effects. For the O$_3$ terminated surfaces (models I and IV), the strongest relaxation occurs again within the Fe bilayer, whereas the

O$_3$-surface layer shows only a modest inward relaxation. The migration of an Fe atom from the second to the first Fe bilayer leaves the near-surface distances unchanged, but significantly reduces the expansion of the distance between the Fe$_3$ layer and its oxygen underlayer. The ferryl-terminated surface (model V) shows weaker relaxation in the FeO layer and of the Fe-O$_3$ distance and again a flattening of the first Fe bilayer.

C. Surface electronic structure

The electronic densities of states for the stable Fe$_2$O$_3$(0001) surfaces are shown in Fig. 5 for GGA calculations and in Fig. 6 for GGA+U calculations. These results should be compared with the bulk DOS shown in Figs. 4 and 9 of Ref. 6. In their nearly octahedral environment in the corundum structure, the $3d$ states of Fe approximately split into bonding and antibonding e_g states, and nonbonding t_{2g} orbitals (see Sec. III, Fig. 3). The degree of hybridization between the Fe-d and the O-$2p$ orbitals is strongly influenced by on-site correlations. In the GGA the Fe-e_g states hybridize strongly with the O-$2p$ states, and in the bulk only a narrow gap of about 0.3 eV exists between the occupied majority t_{2g} band and the empty minority e_g states. At the (0001) surface this narrow gap closes irrespective of the surface termination, i.e., all surfaces are predicted to become
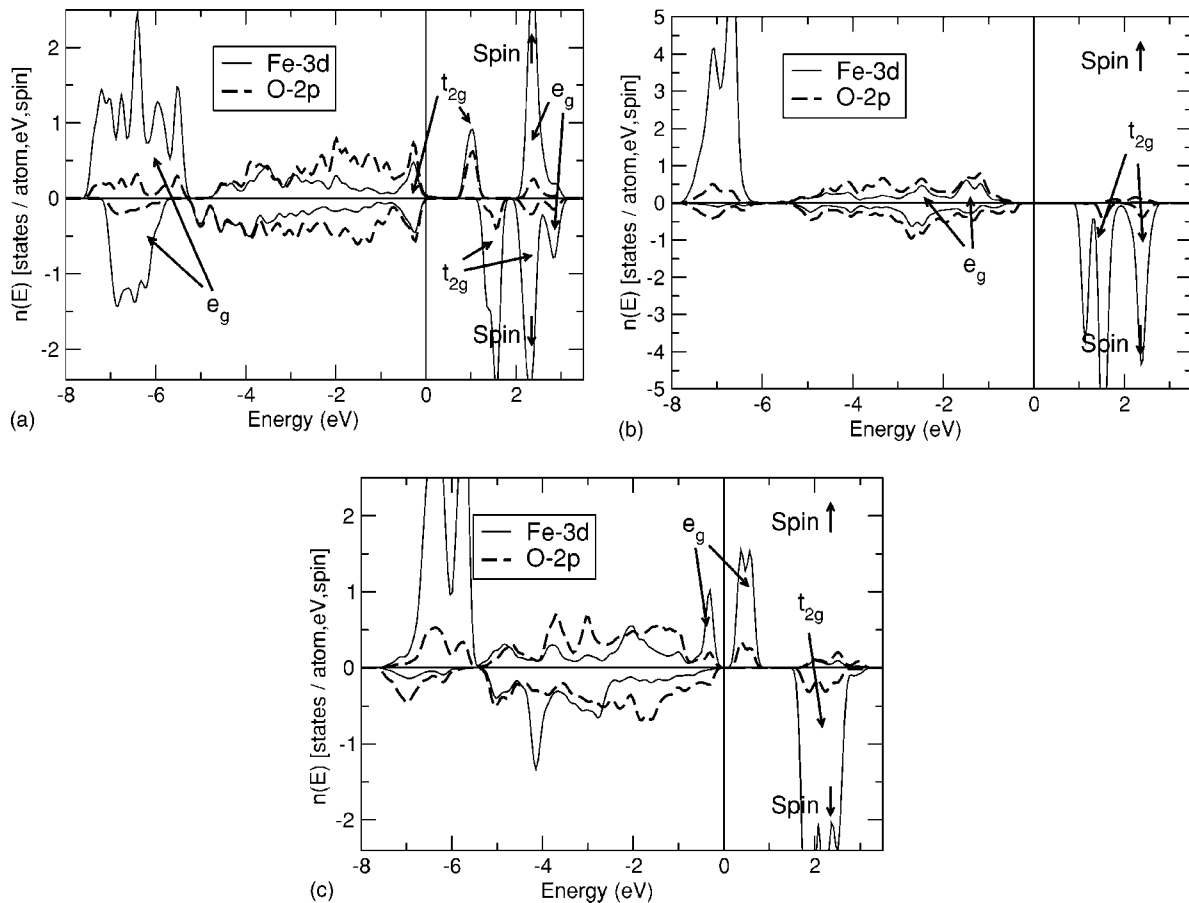
FIG. 6. Electronic densities of states in the near-surface layers (those printed boldface) for the $\cdots$-$FeO_3Fe_3O_3$terminated (a), the $\cdots$-Fe_2O_3Fe terminated (b), and the $\cdots$-Fe_2O_3FeO terminated (c) Fe_2O_3-(0001) surfaces from GGA+U calculations

metallic. For the bulklike $\cdots$-$Fe_2O_3Fe_2O_3$ (model I) and the reconstructed $\cdots$-$FeO_3Fe_3O_3$ (model IV) terminated surfaces the increased oxidation state of the Fe atoms near the surface leads to a pronounced shift of the Fe-d states to lower binding energies and to a strong reduction of the exchange splitting (see also the following subsection on the magnetic surface properties). Without the reconstruction, these effects are even more pronounced.

For the $\cdots$-$FeO_3Fe_3O_3$ terminated surface (model IV), the t_{2g} band near the Fermi level is split for both majority and minority states and partially shifted above the Fermi level (but remember our cautionary remarks concerning the t_{2g}/e_g decomposition and the distortion of the octahedral symmetry induced by the surface relaxation). On the Fe-terminated surface with a reduced Fe content in the top layer, the coordination of the surface Fe atom is very different from the octahedral environment in the bulk. As a result of the reduced coordination the local Fe-d-DOS shows two narrow spin-split bands of mixed t_{2g}/e_g character and a nonbonding e_g band just below E_F. The surface is metallic, but with a low DOS at E_F [see Fig. 5(a)]. On the ferryl-terminated $\cdots$-Fe_2O_3FeO (model V) surface the Fe atom has tetrahedral coordination which implies that the spin-split e_g states are located around the Fermi level, whereas the antibonding t_{2g} are shifted above the Fermi level [see Fig. 5(c)]. In the oxygen-DOS the signatures of the FeO termination are an

increased oxygen-DOS at E_F and sharp structures at binding energies of about −2 eV. This surface is metallic with a high DOS at E_F.

In the GGA+U case, the strong on-site repulsion shifts the occupied e_g and t_{2g} states to higher binding energies and strongly reduces the O-2p-Fe-3d hybridization—there is practically no hybridization with the t_{2g} states any more. The unoccupied e_g states are shifted away from the Fermi level towards higher energy, increasing the width of the energy gap. For the oxygen-terminated surfaces [models I, IV, see Fig. 6(a)] the large surface-induced d-band shifts towards lower binding energies are mainly responsible for their destabilization. The characteristic features of this surface are the gap states of t_{2g} character and the minority component of the e_g states of the lower edge of the valence band (see also the following subsection on magnetic surface properties). For the Fe-terminated $\cdots$-Fe_2O_3Fe (model III) surface, the electronic DOS at the surface differs from that in the bulk mostly by a pronounced narrowing of the Fe-derived bands resulting from the reduced coordination of the Fe atoms. Due to the different symmetry of the Fe environment, the t_{2g} states show a strong exchange splitting. The surface remains semiconducting, with a modest reduction of the gap width [model III—see Fig. 6(b)]. For the ferryl-terminated surface [model V—see Fig. 6(c)]we find a localized surface state on the Fe atoms of e_g symmetry, in accordance with the tetra-

TABLE III. Mean magnetic moments of the first three iron layers for the four relevant surface terminations (AF++−− in-layer ordering). GGA/GGA+U values are given in μ_B. For the nomenclature, see Fig. 1.

	−$Fe_2O_3Fe_2O_3$ (I)	−$FeO_3Fe_3O_3$ (IV)	−Fe_2O_3Fe (III)	−Fe_2O_3FeO (V)
Fe^S			±1.17/±3.94	±1.40/±2.64
Fe^{S-1}	±1.65/±3.28	(+1.70,−2.56,+2.76)/(+2.87,−4.15,+4.15)	±3.36/±4.10	±2.97/±4.11
Fe^{S-3}	±3.48/±4.13	±3.34/±4.10	±3.43/±4.11	±3.48/±4.12
Fe^{S-5}	±3.44/±4.11	±3.34/±4.08		

hedral site symmetry. An empty surface state is located just above the Fermi level.

D. Magnetic surface properties

The layer-magnetic ordering in bulk hematite is AF++−−. The moments between Fe nearest neighbors with short distance (A) are aligned antiparallel whereas the moments between Fe nearest neighbors with long distance (B) couple ferromagnetically.

The magnetic moments of the Fe atoms in the near-surface layers are compiled in Table III. The GGA calculations predict a strong reduction of the magnetic moments at the surface compared to the bulk value of $3.45\mu_B$, irrespective of the surface termination. This agrees with the reduced exchange splitting discussed above. The reduction is about 50% for the oxygen terminated surfaces and even larger for the Fe- and FeO-terminated surfaces. In general, nearest-neighbor Fe atoms within the rumpled Fe layers (see Fig. 1) couple antiferromagnetically. For the reconstructed ⋯-$FeO_3Fe_3O_3$ (model IV) surface with a filled-up Fe^{S-1} layer the magnetic coupling to the added Fe atom is ferromagnetic, while the antiferromagnetic coupling between the Fe atoms present also in the bulk-terminated structure is preserved. Also the coupling of these atoms to the atoms in the Fe-depleted layer remains the same.

The GGA+U calculations predict a much stronger magnetization of the Fe_2O_3 surface. The reduction of the Fe moment is only 20% on the bulklike oxygen terminated surface, and only 10% on the reconstructed oxygen-terminated surface. On the octahedral Fe sites already occupied in the bulk structure, the magnetic moment remains the same as in the bulk whereas the moment on the added Fe atom is reduced by about 30%. On the Fe-terminated surface we find only a marginal reduction of the surface moment by 4%, again this is as expect from the analysis of the surface electronic structure. Only for the ferryl-terminated surface a larger moment

reduction is predicted also by the GGA+U calculations.

E. Core level spectra

The surface-induced Fe-$2p$ core-level shifts have been calculated for four different terminations of the $Fe_2O_3(0001)$ surface, using the approach proposed by Kresse and Köhler.[66] The reference values are the binding energies of the Fe-$2p$ electrons in bulk hematite, a positive value of the surface-induced shift represents a shift to lower binding energies. The results are summarized in Table IV. The layers situated in the middle of the slab show bulklike properties. The results show that on the oxygen-terminated bulklike ⋯-$Fe_2O_3Fe_2O_3$ (model I) surface and on the ferryl terminated (model V) surface the Fe core levels are shifted by ∼−1.2 and ∼−1.6 eV, respectively, to larger binding energies. Adding strong correlations in the GGA+U leads only to a marginal reduction of the core-level shift. For the reconstructed oxygen-terminated surface ⋯-$Fe_2O_3Fe_3O_3$ (model IV) has a substantially weaker shift, but to lower binding energies. For the iron-terminated surface we calculate a minimal shift of only ∼0.2 eV (GGA) and ∼0.3 eV (GGA+U), again to lower binding energies.

The overall trend in the core level shifts for different terminations is similar as calculated by Kresse *et al.*[68] for $V_2O_3(0001)$, but there the core level shifts calculated for the different terminations do not differ as much as for $Fe_2O_3(0001)$. They found the shifts of the vanadyl- (VO) and the bulklike oxygen-terminated surface close together at ∼1 eV, whereas the shift of the vanadium-terminated surface nearly vanishes (0.01 eV).

Core level spectra exist from different experimental sources.[35,76–79] In most cases core-level spectroscopy has been used to estimate the amount of octahedrally and tetrahedrally coordinated Fe in thin films and thus to determine the hematitelike and magnetitelike fractions of the film struc-

TABLE IV. Fe-$2p$ surface core level shifts (in eV) for $Fe_2O_3(0001)$ surfaces calculated for four different terminations. For the bulklike oxygen-terminated −$Fe_2O_3Fe_2O_3$ and the iron-terminated −Fe_2O_3Fe surface both GGA and GGA+U values are reported.

	−$Fe_2O_3Fe_2O_3$ (I)	−$FeO_3Fe_3O_3$ (IV)	−Fe_2O_3Fe (III)	−Fe_2O_3FeO (V)
Fe^S			0.19/0.29	−1.61
Fe^{S-1}	−1.21/−1.08	0.37	−0.03/0.16	−0.06
Fe^{S-3}	−0.03/−0.01	−0.18	−0.02/−0.03	−0.01
Fe^{S-5}	0.07/0.07	−0.35		

ture. A surface-sensitive analysis has been undertaken only by Fujii *et al.*[76] who reported a small shift of the Fe-$2p^{3/2}$ and $2p^{1/2}$ levels to lower binding energies with decreasing thickness of a α-Fe$_2$O$_3$(0001) film and by Chambers and Droubay[79] who reported that the Fe-$2p$ peak energies measured on Fe$_2$O$_3$ films grown on Pt(111) do not show any dependence on the film thickness. Droubay and Chambers[78] measured a reduction of the splitting of the Fe-$2p^{3/2}$ level in the octahedral crystal field into t_{2g} and e_g orbital sets in Fe$_2$O$_3$ films grown on α-Al$_2$O$_3$ with decreasing film thickness, indicating a different site symmetry at the surface. The smallness of the surface-induced shift of the Fe-$2p$ levels to lower binding energies (which is difficult to quantify on the basis of the data published by Fujii *et al.*[76]) or even the complete absence of such a shift[79] excludes the bulklike oxygen terminated and the ferryl-terminated surfaces. Combined with the calculated surface energies and with the theoretical structure data in conjunction with the LEED measurements this supports an Fe termination of the surfaces under UHV conditions.

V. Cr$_2$O$_3$(0001) SURFACES

A. Phase stability and surface structure

The surface energies as a function of the chemical potential of oxygen as calculated for different terminations of the Cr$_2$O$_3$(0001) surface using the GGA and the GGA+U are shown in Fig. 7. The surface energies show the same behavior as for the Fe$_2$O$_3$(0001) surface, but the possibility to oxidize Cr$_2$O$_3$ to Cr dioxide introduces a new facet. At low partial pressures of oxygen where surface oxidation is suppressed, only the Cr-terminated $\cdots$-Cr$_2$O$_3$Cr (model III) surface is found to be stable, in the GGA as well as in the GGA+U. In the GGA, a chromyl-terminated $\cdots$-Cr$_2$O$_3$CrO (model V) surface is stable at values of the chemical potential where the oxidation to CrO$_2$ becomes energetically favored. An oxygen terminated surface can be metastable at even higher partial pressures of oxygen. Hence the sequence Cr-terminated(III) → chromyl-terminated (V) → oxygen- terminated (IV) surfaces agrees with the phase stabilities predicted by the FLAPW calculations of Wang and Smith.[50] In the GGA+U all oxygen-terminated surfaces are strongly disfavored. The range of stability of a chromyl-terminated surface is also shifted to strongly oxidizing conditions such that this surface is at best metastable against the formation of Cr dioxide. A Cr-terminated $\cdots$-Cr$_2$O$_3$Cr$_2$ (model II) surface with a full bulklike coverage of the top Cr layer is found to be unstable under any condition. Experimental studies of the Cr$_2$O$_3$(0001) surface up to now only reported a chromium termination,[42,45] in agreement with the phase stabilities predicted by our GGA+U calculations. In their combined EELS and LEED study of Cr$_2$O$_3$(0001) surfaces, Bender *et al.*[80] reported a diffuse (1×1) LEED pattern at room temperature, the appearance of a ($\sqrt{3} \times \sqrt{3}$)$R30°$ pattern at 180 K, and a return to a sharp (1×1) pattern at about 130 K. This was interpreted as indicating an order/disorder transition, followed by an order/order transition at lower temperature and associated with different occupancies of the threefold hol-
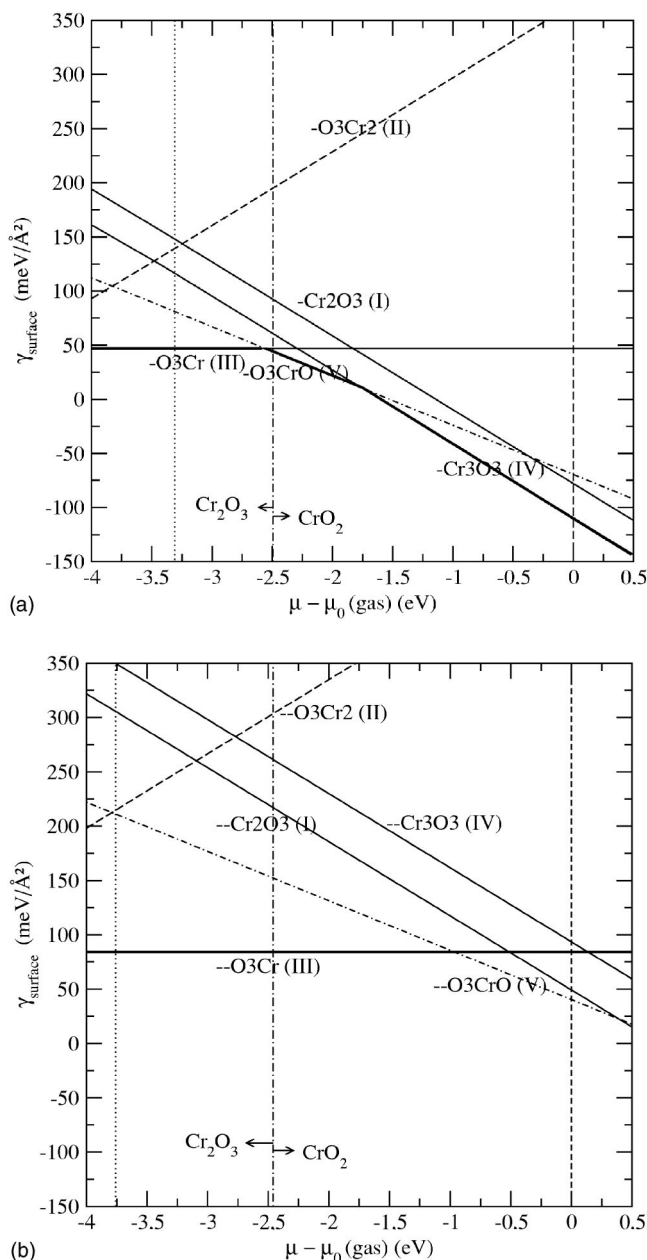

FIG. 7. (a) GGA derived surface energies of the different terminations plotted against oxygen chemical potentials. (b) GGA+U derived surface energies plotted against oxygen chemical potentials. The dotted and dashed vertical lines mark the upper and lower limits of the chemical potential as given by the condensation of molecular oxygen at the surface and the reduction of chromia to metallic Cr. The dot-dashed vertical lines mark the value of the chemical potential where the oxidation of Cr$_2$O$_3$ to CrO$_2$ becomes energetically favored. GGA+U calculations for CrO$_2$ have been performed with U=5 eV, equal to Cr$_2$O$_3$.

lows in the O$_3$ layer by Cr atoms. In contrast, Maurice *et al.*[45] found no indication of structural disorder in their STM images. However, the STM images can be interpreted in terms of a statistical site occupancy of the Cr ions in the surface sites, assuming that surface diffusion takes place already at room temperature.

TABLE V. Surface relaxation for the four relevant terminations of the $Cr_2O_3(0001)$ surface. The relaxations of the first four ML are given in % of the bulk interlayer distances. The bulk interlayer Cr-O distance is 0.94/0.95 Å(GGA/GGA+U), the intra layer Cr-Cr distance is 0.38/0.41 Å.

	···-Cr_2O_3CrO (V)		···-Cr_2O_3Cr (III)				···-$Cr_2O_3Cr_2O_3$ (I)		···-$CrO_3Cr_3O_3$ (IV)	
	GGA	GGA+U	GGA	GGA+U	HF (calc)[a]	Exp.[b]	GGA	GGA+U	GGA	GGA+U
O-Cr	−27	−25								
Cr-O_3^S	−1.2	−1	−62	−60	−50	−58				
O_3^S-Cr^{S-1}	+13	+12	+10	+12	3.3	0	+13	+3.3	+2.0	+4.5
Cr^{S-1}-Cr^{S-1}	−48	−43	−41	−44	0[c]	−36	+9.2	+29	+13	+4.4
Cr^{S-1}-O_3^{S-2}	−1.1	+0.2	+6.5	+9.2	0[c]	+17	−29	−32	−28	−27

[a]Ref. 39.
[b]Ref. 42 (erratum).
[c]Kept fixed at bulk spacing.

The changes in the interlayer distances of the relaxed slabs for the five different surface terminations are reported in Table V. The chromium-terminated surface shows strong relaxations in the surface layer (∼60%) and in the first sublayer (∼40%), in excellent agreement with experiment.[42] The sublayer relaxations of the chromyl-terminated surface are very similar to the chromium-terminated surface. The difference between GGA and GGA+U calculations is small. The oxygen-terminated surface show weak surface relaxations, with larger discrepancies between GGA and GGA+U. Hence only the Cr-terminated surface is compatible with the LEED data.

Previously, Rehbein *et al.*[39] performed a HF study of the structure of the Cr-terminated Cr_2O_3 surface, using the method applied by Catti *et al.*[12] to bulk chromia. Only the top Cr-O_3 and O_3-Cr_2 interlayer distances have been allowed to relax. Considering the drastic differences in the HF and GGA(GGA+U) predictions for the electronic structure of chromia, the good agreement of the calculated interlayer relaxations [surface layer: −50% (HF), −60% (GGA+U), subsurface layer: +3.3% (HF), +12% (GGA+U)] is surprising. This confirms our conclusion that the mechanism leading to the large surface relaxations is largely electrostatic in nature. Rehbein *et al.* also emphasize that a detailed analysis reveals no change in the character of the Cr-O bonds at the surface. Altogether, the excellent agreement of the calculated surface relaxation with the LEED analysis and the predicted stability of the Cr-terminated surface even a wide range of oxygen partial pressures confirm that GGA+U provides a correct description of the chromia surface.

B. Surface electronic structure

Electronic densities of states were calculated for the stable (disregarding the oxidation to CrO_2) surface terminations, using the GGA and the GGA+U (see Figs. 8 and 9). As for the $Fe_2O_3(0001)$ surface, GGA calculations predict all surfaces to be metallic or semi-metallic. The surface-induced band narrowing tends to broaden the gap between the hybridized O-2p-Cre_g band at higher binding energy and the Fe-t_{2g} bands around the Fermi level, which exist already in the bulk. For the reconstructed oxygen terminated ···-$CrO_3Cr_3O_3$ (model IV) surface [see Fig. 8(a)] the increased oxidation state of Cr leads to a strong shift of the Cr-t_{2g} bands to lower binding energies and a depletion of the majority band. Due to the incomplete band filling, the surface is predicted to be metallic with a high DOS at E_F. The strong d-band shift reflects the high energy cost for stabilizing this surface. For the chromyl-terminated (model V) surface we observe a similar shift of the d bands to lower binding energies, with a half-occupied e_g band and an empty t_{2g} band in the majority states, and a high DOS at E_F in accordance with the tetrahedral site symmetry of the Cr atoms [see Fig. 8(c)]. The minority states are shifted above the Fermi level, but the exchange splitting is strongly reduced so that the Cr-surface moment is quenched even more strongly as for the oxygen-terminated surface (see also the following subsection). A further signature of the chromyl-termination are the strong structures in the oxygen DOS at binding energies of −2.5 and −4 eV. For the stable Cr-terminated ···-Cr_2O_3Cr (model III) surface the Fermi level falls into a narrow gap between the majority states with e_g and t_{2g} character, no minority e_g states are occupied. Hence for the Cr-terminated surface the magnetism of the surface should not differ appreciably from that in the bulk.

In the GGA+U, the increased exchange splitting leads to a substantial O-2p-Fe-3d hybridization even at the surface, and the surface remains semiconducting at all terminations. For the reconstructed ···-$CrO_3Cr_3O_3$ terminated (model IV) surface the electronic surface DOS is mostly bulklike, except for an exchange-split surface state of t_{2g} character placing the empty spin-up state right into the center of the bulk-gap [see Fig. 9(a)]. The band gap is reduced from 2.6 eV to about 1.2 eV for a Cr-terminated surface [model III—see Fig. 9(b)] and to about 1 eV for the CrO-terminated case [model V—see Fig. 9(c)]. This is in good agreement with weak loss peaks in the EELS spectrum at 1.2 and 1.4 eV assigned to d-d excitations in the Cr ions at the (0001) surface.[40,80,81] For the chromyl-terminated surface the states close to the Fermi level are of e_g character, in accordance with the tetrahedral site symmetry of the Cr atoms.

C. Surface magnetism

The layerwise magnetic ordering in Cr_2O_3 is AF+−+−, so that all moments between two Cr nearest neighbors, re-
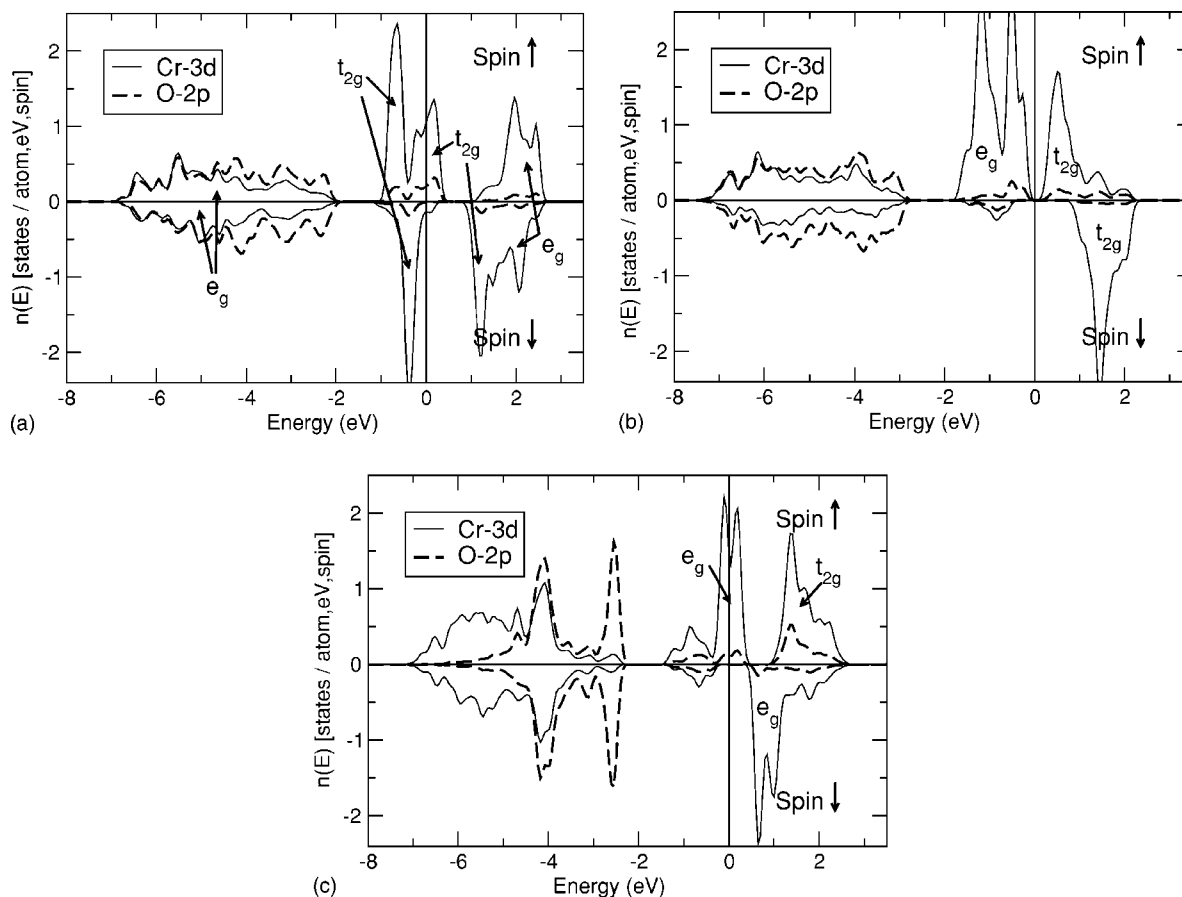
FIG. 8. Electronic densities of states of the top layers (marked by boldface printing) of the $\cdots$-CrO$_3$Cr$_3$O$_3$ terminated (a), the $\cdots$-Cr$_2$O$_3$Cr terminated (b), and the $\cdots$-Cr$_2$O$_3$CrO terminated (c) surfaces of chromia from GGA calculations.

gardless their distance, have antiparallel alignment. The magnetic moments calculated for the near-surface chromium layers (see Table VI) are reduced compared to the bulk, similar as reported for the Fe$_2$O$_3$(0001) surface. In the GGA, the strongest demagnetization (about 70%) is predicted for the chromyl-terminated surface (model V). For the bulklike (model I) and reconstructed oxygen-terminated (model IV) surfaces, the magnetic moments at the surface are reduced by 44 and 17%, respectively. On the reconstructed surface, the moments in the Cr-depleted subsurface layer are also reduced. The Cr atom transferred to the topmost Cr^{S-1} layer conserves the orientation of its magnetic layer so that in the filled-up Cr^{S-1} layer we find two spin-up and one spin-down moment, whereas in the depleted Cr^{S-3} layer all moments have spin-down orientation. For the Cr-terminated surface both the GGA and the GGA+U calculation agree on the full value of the magnetic moment also at the surface. For the other surface terminations, the GGA+U calculations point to a similar, but slightly smaller reduction of the magnetic moments as the GGA.

D. Core level spectra

Calculated Cr-2p core level shifts for four different terminations of the Cr$_2$O$_3$(0001) surface are shown in Table VII. Again, the $-$Cr-terminated (model III) surface shows the

weakest, the CrO termination (model V) the strongest shift. In general, the values do not differ as much as for the different Fe$_2$O$_3$(0001) surface terminations. Experimental spectra are all taken at UHV conditions and the surface was therefore chromium terminated. From Cr$_2$O$_3$(0001) grown on Pt(111), core level spectra of different coverages show a shift in the position of the Cr-2p peak by "at most a few tenths of an eV" to lower binding energies as the film thickness increases from 1 to 5 ML (at this thickness the position of the core level is already converged to that in the bulk). Again, this is in reasonable agreement with the DFT results for the Cr-terminated surface. Spectra of oxygen-terminated surfaces are not available, since they cannot be stabilized even in oxygen-rich environments.

VI. CONCLUSIONS

We have presented a detailed analysis of the structural, electronic, and magnetic properties of the polar (0001) surfaces of α-Fe$_2$O$_3$ (hematite) and of α-Cr$_2$O$_3$ (eskolaite or chromia), with particular attention to the effects of strong electronic correlations. The starting point of our investigations was an analysis of correlation effects in bulk Cr$_2$O$_3$, supplementing our earlier study of hematite.[6] We have shown that whereas DFT calculations at the GGA level predict a narrow energy gap of only 1.2 eV between the major-
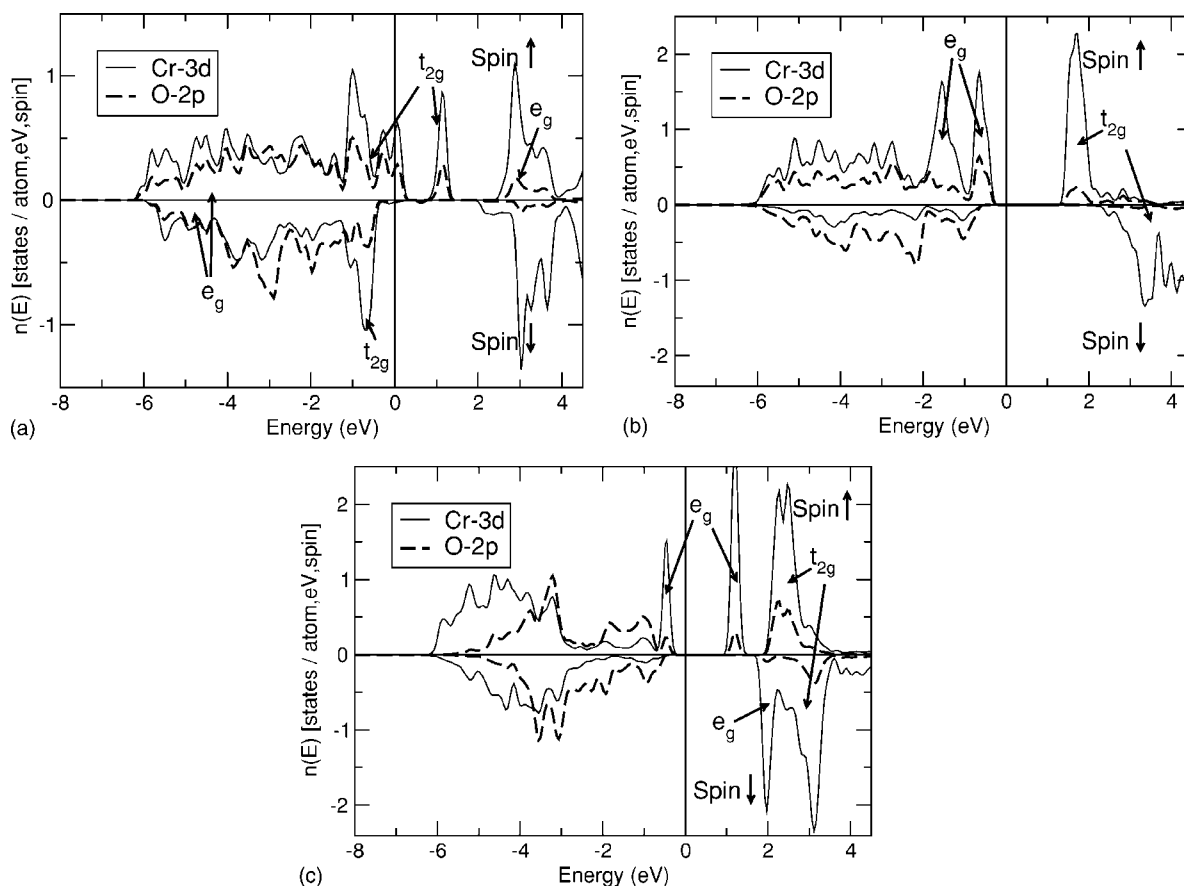
FIG. 9. Electronic densities of states of the top layers (marked by boldface printing) of the $\cdots$-$CrO_3Cr_3O_3$ terminated (a), the $\cdots$-$Cr_2O_3O_3Cr$ terminated (b), and the $\cdots$-Cr_2O_3CrO terminated (c) surfaces of chromia from GGA+U calculations.

ity Cr-t_{2g} and the minority Cr-e_g states (hence classifying chromia as a Mott-Hubbard d-d insulator), GGA+U calculations with an on-site Coulomb repulsion of $U=5$ eV predict a stronger Cr-d-O-p hybridization and a wider gap of 2.6 eV between a valence-band edge of strongly mixed Cr -t_{2g}-O-p character and the lowest conduction band of Cr-e_g character. This leads to the conclusion, supported by photoemission and inverse photoemission experiments, that Cr_2O_3, represents an intermediate case between a charge transfer and a Mott-Hubbard insulator. In particular, we note—as already for Fe_2O_3—that the on-site Coulomb repulsion modifies the character of the "frontier orbitals" and hence can be expected to have a decisive influence on the surface chemical reactivity.

The investigations of the (0001) surfaces lead to a rather complex picture of the influence of strong electronic correlations on the surface properties: On one hand, the oxygen-terminated surfaces for both Fe_2O_3 and Cr_2O_3 are energetically strongly disfavored relative to the metal-terminated surfaces if the on-site Coulomb repulsion is taken into account, on the other hand, the strong geometrical relaxation of the surfaces is hardly influenced by correlation effects. Within the entire allowed range of partial pressures of oxygen, the Fe- and Cr-terminated surfaces with only one-third of the sites in the surface layer occupied by metal atoms are predicted to be stable (in the bulk two thirds of the octahedral sites are occupied by TM atoms). Only for Fe_2O_3, a ferryl-terminated surface could exist under strongly oxidizing conditions. For both oxides, this is in accordance with the most recent STM and LEED data. The destabilization of any form of oxygen terminations is clearly a consequence of the strong on-site correlations: For the oxygen- and TM-O-terminated surfaces, the increased oxidation state of the transition-metal ions leads to a shift of the TM-d bands to-

TABLE VI. Magnetic moment absolute mean values (antiferromagnetic in-layer ordering) of the first three chromium layers for the four relevant terminations. GGA/GGA+U values are indicated in μ_B. For $-Cr_3O_3$, all three in-layer values are indicated.

	$-Cr_2O_3Cr_2O_3$ (I)	$-CrO_3Cr_3O_3$ (IV)	$-Cr_2O_3Cr$ (III)	$-Cr_2O_3CrO$ (V)
Cr^S			$\pm2.68/\pm3.04$	$\pm0.89/\pm1.15$
Cr^{S-1}	$\pm1.53/\pm1.65$	$(+1.72,-2.56,+2.72)/(+2.52,-2.96,+2.83)$	$\pm2.63/\pm3.01$	$\pm2.60/\pm2.99$
Cr^{S-3}	$\pm2.63/\pm3.00$	$-2.21/-2.36$	$\pm2.67/\pm3.01$	$\pm2.65/\pm3.01$
Cr^{S-5}	$\pm2.68/\pm3.00$	$\pm2.38/\pm2.90$		

TABLE VII. Surface-induced core level shifts for $Cr_2O_3(0001)$ in four different terminations, calculated using the GGA. For the bulklike oxygen and the chromium termination, GGA/GGA$+U$ values are reported.

	$-Cr_2O_3Cr_2O_3$ (I)	$-CrO_3Cr_3O_3$ (IV)	$-Cr_2O_3Cr$ (III)	$-Cr_2O_3CrO$ (V)
Cr^S			0.40/0.40	-0.97
Cr^{S-1}	$-0.67/-0.85$	-0.63	0.02/0.33	-0.14
Cr^{S-3}	$-0.18/-0.64$	-0.95	$-0.01/0.11$	-0.13
Cr^{S-5}	$-0.01/-0.16$	-0.38		

wards lower binding energies. On both the Fe_2O_3 and the Cr_2O_3 surfaces the majority d band is partly shifted above E_F and depleted. The energetic cost for the d-band shift and the electron transfer from the transition-metal to oxygen is much higher if the on-site Coulomb repulsions leading to the correct d-band position in the bulk are taken into account. The surface properties predicted from GGA and GGA$+U$ calculations are drastically different: the GGA predicts metallic surfaces with strongly quenched magnetic moments, while the GGA$+U$ predicts the persistence of an insulating gap and a much lower reduction of the surface moments. Hence an investigation of the chemical reactivity of the surfaces via the adsorption of small probe molecules should lead to a conclusive picture of the role of strong electronic correlation in hematite and chromia surfaces.

The conclusion that under realistic values of the partial pressures of oxygen both both Fe_2O_3 and Cr_2O_3 only a TM-terminated surface is stable agrees with experimental observations on the geometric structure and the electronic properties. The comparison of the conflicting STM studies[5,49] shows that the preparation conditions may be of decisive importance for the experimental observations.

*Email address: juergen.hafner@univie.ac.at

[1] W. Geus, Appl. Catal. **25**, 313 (1986).

[2] J. Kennedy and K. Freese, J. Electrochem. Soc. **125**, 709 (1978).

[3] T. Uozumi, K. Okada, and A. Kotani, J. Electron Spectrosc. Relat. Phenom. **78**, 103 (1996).

[4] A. Rohrbach, J. Hafner, and G. Kresse, Phys. Rev. B **69**, 075413 (2004).

[5] X. G. Wang, W. Weiss, S. K. Shaikhutdinov, M. Ritter, M. Petersen, F. Wagner, R. Schlögl, and M. Scheffler, Phys. Rev. Lett. **81**, 1038 (1998).

[6] G. Rollmann, A. Rohrbach, P. Entel, and J. Hafner, Phys. Rev. B **69**, 165107 (2004).

[7] A. Fujiimori, M. Saeki, N. Kimizuka, M. Taniguchi, and S. Suga, Phys. Rev. B **34**, 7318 (1986).

[8] R. J. Lad and V. E. Henrich, Phys. Rev. B **39**, 13 478 (1989).

[9] J. Badro, G. Fiquet, V. V. Struzhkin, M. Somayazulu, H. Mao, G. Shen, and T. L. Bihan, Phys. Rev. Lett. **89**, 205504 (2002).

[10] M. P. J. Punkkinen, K. Kokko, W. Hergert, and I. J. Väyrynen, J. Phys.: Condens. Matter **11**, 2341 (1999).

[11] L. M. Sandratskii, M. Uhl, and J. Kübler, J. Phys.: Condens. Matter **8**, 983 (1996).

[12] M. Catti, G. Sandrone, G. Valerio, and R. Dovesi, J. Phys. Chem. Solids **57**, 1735 (1996).

[13] I. Pop, M. Andrecut, I. Burda, O. Pop, I. Ivan, I. Nazarenco, and C. Oprea, Mater. Chem. Phys. **47**, 85 (1997).

[14] I. Pop, M. Andrecut, I. Burda, C. Oprea, and C. Andrecut, J. Mater. Sci. Lett. **16**, 2052 (1997).

[15] A. Y. Dobin, W. Duan, and R. M. Wentzcovitch, Phys. Rev. B **62**, 11 997 (2000).

[16] R. Zimmermann, P. Steiner, and S. Hüfner, J. Electron Spectrosc. Relat. Phenom. **78**, 49 (1996).

[17] S. Mochizuki, Phys. Status Solidi A **41**, 591 (1977).

[18] J. Crawford and R. West, J. Appl. Phys. **35**, 2413 (1964).

[19] J. Zaanen, G. Sawatzky, and J. W. Allen, Phys. Rev. Lett. **55**, 418 (1985).

[20] D. Adler, Solid State Phys. **21**, 83 (1968).

[21] C. W. Searle and G. W. Dean, Phys. Rev. B **1**, 4337 (1970).

[22] L. M. Corliss, J. Appl. Phys. **36**, 1099 (1965).

[23] L. Pauling and S. Hendricks, J. Am. Chem. Soc. **47**, 781 (1925).

[24] A. Fujimori, M. Saeki, N. Kimizuka, M. Taniguchi, and M. Suga, Phys. Rev. B **39**, 13 478 (1989).

[25] F. Ciccacci, L. Braicovich, E. Puppin, and E. Vescovo, Phys. Rev. B **44**, 10 444 (1991).

[26] X. Li, L. Liu, and V. E. Henrich, Solid State Commun. **84**, 1103 (1992).

[27] T. Uozumi, K. Okada, A. Kotani, R. Zimmermann, P. Steiner, S. Hüfner, Y. Tezuka, and S. Shin, J. Electron Spectrosc. Relat. Phenom. **83**, 9 (1997).

[28] K. Wolter, D. Scarano, J. Fritsch, H. Kuhlenbeck, A. Zecchina, and H.-J. Freund, Chem. Phys. Lett. **320**, 206 (2000).

[29] S. L. Dudarev, A. I. Liechtenstein, M. R. Castell, G. A. D. Briggs, and A. P. Sutton, Phys. Rev. B **56**, 4900 (1997).

[30] S. L. Dudarev, G. A. Botton, S. Y. Savrasov, C. J. Humphreys, and A. P. Sutton, Phys. Rev. B **57**, 1505 (1998).

[31] O. Bengone, M. Alouani, P. Blöchl, and J. Hugel, Phys. Rev. B **62**, 16 392 (2000).

[32] A. I. Liechtenstein, V. I. Anisimov, and J. Zaanen, Phys. Rev. B **52**, R5467 (1995).

[33] V. I. Anisimov and F. Aryasetiawan, J. Phys.: Condens. Matter **9**, 767 (1997).

[34] Q. Guo, P. H. McBreen, and P. J. Moller, Surf. Sci. **423**, 19 (1999).

[35] S. A. Chambers, Y. J. Kim, and Y. Gao, Surf. Sci. Spectra **5**, 219 (1998).

[36] P. J. Moller, Q. Guo, and L. Gui, Thin Solid Films **281**, 76 (1996).

[37] N. G. Condon, F. M. Leibsle, A. R. Lennie, P. W. Murray, T. M. Parker, D. J. Vaughan, and G. Thornton, Surf. Sci. **397**, 278 (1998).

[38] G. S. Herman, E. P. McDaniel, and S. A. Joyce, J. Electron Spectrosc. Relat. Phenom. **101**, 433 (1999).

[39] C. Rehbein, N. M. Harrison, and A. Wander, Phys. Rev. B **54**, 14 066 (1996).

[40] J. A. Mejias, V. Staemmler, and H.-J. Freund, J. Phys.: Condens. Matter **11**, 7881 (1999).

[41] Q. Guo, L. Gui, P. J. Moller, and K. Binan, Appl. Surf. Sci. **92**, 513 (1996).

[42] F. Rohr, M. Bäumer, H.-J. Freund, J. A. Mejias, V. Staemmler, S. Müller, L. Hammer, and K. Heinz, Surf. Sci. **372**, L291 (1997).

[43] L. Zhang, M. Kuhn, and U. Diebold, Surf. Sci. **375**, 1 (1997).

[44] P. Robbert, H. Geisler, C. Centrice, J. van Eck, S. Chaturvedi, J. Rodriguez, M. Kuhn, and U. Diebold, J. Vac. Sci. Technol. A **16**, 990 (1998).

[45] V. Maurice, S. Cadot, and P. Marcus, Surf. Sci. **458**, 195 (2000).

[46] W. Mackrodt, R. Davey, and S. Black, J. Cryst. Growth **80**, 441 (1987).

[47] E. Wassermann, J. R. Rustad, A. R. Felmy, B. P. Hay, and J. W. Halley, Surf. Sci. **385**, 217 (1997).

[48] I. Lado-Tourino and F. Tsobnang, Comput. Mater. Sci. **17**, 243 (2000).

[49] S. Chambers and S. Yi, Surf. Sci. **439**, L785 (1999).

[50] X. Wand and J. R. Smith, Phys. Rev. B **68**, 201402 (2003).

[51] G. Kresse and D. Joubert, Phys. Rev. B **59**, 1758 (1999).

[52] G. Kresse and J. Hafner, Phys. Rev. B **47**, 588 (1993).

[53] G. Kresse and J. Hafner, Phys. Rev. B **49**, 14 251 (1994).

[54] G. Kresse and J. Furthmüller, Phys. Rev. B **54**, 11 169 (1996).

[55] G. Kresse and J. Furthmüller, Comput. Mater. Sci. **6**, 15 (1996).

[56] J. Perdew and A. Zunger, Phys. Rev. B **23**, 5048 (1981).

[57] J. Perdew, J. Chevary, S. Vosko, K. Jackson, M. Pederson, D. Singh, and C. Fiolhais, Phys. Rev. B **46**, 6671 (1992).

[58] S. Vosko, L. Wilk, and M. Nusair, Can. J. Phys. **58**, 1200 (1980).

[59] P. Blöchl, Phys. Rev. B **50**, 17 953 (1994).

[60] G. Kresse and D. Joubert, Phys. Rev. B **59**, 1758 (1999).

[61] D. M. Wood and A. Zunger, J. Phys. A **18**, 1343 (1985).

[62] D. D. Johnson, Phys. Rev. B **38**, 12 807 (1988).

[63] P. Pulay, Chem. Phys. Lett. **73**, 393 (1980).

[64] H. Monkhorst and J. D. Pack, Phys. Rev. B **13**, 5188 (1976).

[65] A. Eichler, J. Hafner, and G. Kresse, J. Phys.: Condens. Matter **8**, 7659 (1996).

[66] L. Köhler and G. Kresse, Phys. Rev. B (to be published).

[67] A. Rohrbach, J. Hafner, and G. Kresse, J. Phys.: Condens. Matter **15**, 979 (2003).

[68] G. Kresse, S. Surnev, J. Schoiswohl, and F. Netzer, Surf. Sci. **555**, 118 (2004).

[69] K. Reuter and M. Scheffler, Phys. Rev. B **65**, 035406 (2002).

[70] L. Finger and R. Hazen, J. Appl. Phys. **51**, 5362 (1980).

[71] Y. Sato and S. Akimoto, J. Appl. Phys. **50**, 5285 (1979).

[72] J. Coey and G. Sawatzky, J. Phys. C **4**, 2386 (1971).

[73] E. Kren, P. Szabo, and G. Konczos, Phys. Lett. **19**, 103 (1965).

[74] A. Lennie, N. Condon, F. Leibsle, P. Murray, G. Thornton, and D. Vaughan, Phys. Rev. B **53**, 10 244 (1996).

[75] A. Barbieri, W. Weiss, M. van Hove, and G. Somorjai, Surf. Sci. **302**, 259 (1994).

[76] T. Fujii, D. Alders, F. C. Voogt, T. Hibma, B. T. Thole, and G. A. Sawatzky, Surf. Sci. **366**, 579 (1996).

[77] T. Fujii, F. M. F. de Groot, G. A. Sawatzky, F. C. Voogt, T. Hibma, and K. Okada, Phys. Rev. B **59**, 3195 (1999).

[78] T. Droubay and S. A. Chambers, Phys. Rev. B **64**, 205414 (2001).

[79] S. A. Chambers and T. Droubay, Phys. Rev. B **64**, 075410 (2001).

[80] M. Bender, D. Ehrlich, I. N. Yakovin, F. Rohr, M. Bäumer, H. Kuhlenbeck, H. J. Freund, and V. Staemmler, J. Phys.: Condens. Matter **7**, 5289 (1995).

[81] M. Bender, I. N. Yakovkin, and H.-J. Freund, Surf. Sci. **365**, 394 (1996).